文章编号: **DOI:** 10.15541/jim20230501

Effect of Pb^{2+} on the Luminescent Performance of $CsPbBr_3$ Perovskite Quantum Dots Embedded Borosilicate Glass

YUE Zihao[1,2], YANG Xiaotu[1], ZHANG Zhengliang[1], DENG Ruixiang[1], ZHANG Tao[1], SONG Lixin[1,2]

(1. Shanghai Institute of Ceramics, Chinese Academy of Sciences, Shanghai 200050, China; 2. School of Physical Science and Technology, ShanghaiTech University, Shanghai 201210, China)

Abstract: Encapsulation of perovskite $CsPbBr_3$ quantum dots (PQDs) within borosilicate glass markedly improves the stability of these PQDs, thereby expanding their applicability in sectors such as in the context of light emitting diode (LED) lighting and display. However, this encapsulation process within the glass has the unintended consequence of reducing both the photoluminescence (PL) intensity and photoluminescence quantum yields (PLQY) of the PQDs. This research elucidates the impact of thermal annealing temperature and Pb^{2+} content on the structural characteristics of $CsPbBr_3$ perovskite quantum dots embedded glass (PQDs@glass), leading to a remarkable amplification in the emission intensity and an impressive PLQY of up to 95.6% for PQDs@glass. Concurrently, this investigation has successfully accomplished precise size-controlled synthesis of perovskite quantum dots within a borosilicate glass matrix. The obtained results reveal a well-defined size distribution of PQDs, with an average diameter of approximately 10 nm. Remarkably, over 86% of the particles fall within the narrow size range of 6-14 nm. Notably, these PQDs exhibit exceptional stability, as evidenced by their ability to retain an extraordinary 98.9% of the initial emission intensity following ten consecutive thermal cycles spanning from ambient temperature to 200 ℃. Finally, in order to verify its applicability in the domains of LED lighting and displays, the PQDs@glass powder obtained from this study was blended with polydimethylsiloxane (PDMS), yielding exemplary LED devices exhibiting an exceptional color gamut range surpassing 110% of the standard RGB (sRGB) color space. This lays the groundwork for the scalable synthesis of PQDs@glass and paves the way for its utilization in the realm of LED device technology.

Key words: $CsPbBr_3$; Pb^{2+}; LED; QDs; borosilicate glass

Light emitting diode (LED) applications in the fields of lighting and display have witnessed rapid growth alongside the progression of time, imposing heightened demands on LED performance[1-3]. $CsPbBr_3$ QDs were considered an ideal material for LED device fabrication due to their high PL intensity, PLQY, and color purity[4-6]. However, the stability of colloidal $CsPbBr_3$ QDs was relatively poor, limiting their application in the fields of LED lighting and display. To address this issue, various strategies including ion doping[7-10], surface passivation[11-12], and encapsulation[13-16] were extensively explored by researchers to optimize and enhance the stability of $CsPbBr_3$ QDs. Although these approaches partially improved the stability of $CsPbBr_3$ QDs, they could only mitigate external factors' corrosion on QDs, resulting in limited protection efficacy in practical applications. Subsequently, the strategy of encapsulating $CsPbBr_3$ QDs in glass to form glass-ceramic was discovered by researchers, which effectively isolated $CsPbBr_3$ QDs from the external environment and significantly enhanced their stability[17-21]. This approach provided an ideal solution for improving the stability of $CsPbBr_3$ QDs.

The use of $CsPbBr_3$ QDs coated with glass encapsulation, while enhancing their stability, presents various challenges. Firstly, although glass is a transparent material, inevitable scattering and refraction effects occur, resulting in the attenuation of emitted light intensity and color purity of $CsPbBr_3$ QDs. Secondly, due to its amorphous nature, the internal structure of glass is

Received date: 2023-10-30; **Revised date:** 2023-12-05

Biography: YUE Zihao (1994–), male, Master candidate. E-mail: yuezh@shanghaitech.edu.cn
岳仔豪(1994–)，男，硕士研究生. E-mail: yuezh@shanghaitech.edu.cn
Corresponding: DENG Ruixiang, lecturer. E-mail: dengruixiang@mail.sic.ac.cn; ZHANG Tao, professor. E-mail: tzhang@mail.sic.ac.cn
邓瑞翔，助理研究员. E-mail: dengruixiang@mail.sic.ac.cn; 张 涛，研究员. E-mail: tzhang@mail.sic.ac.cn

complex, necessitating precise manipulation by researchers to provide an optimal environment for the formation of $CsPbBr_3$ QDs within the $CsPbBr_3$ QDs@glass system. Furthermore, the composition of $CsPbBr_3$ QDs also exerts an influence on the glass structure. It has been demonstrated that an abundance of Cs promotes the formation of $CsPbBr_3$ QDs within the glass matrix. However, an excessive amount of Cs^+ disrupts the three-dimensional network structure of glass[22-23], a characteristic observed in alkali metal elements. Another approach involves substituting PbBr with PbO[24], which significantly reduces volatility during solvation, enhances the luminescent intensity of $CsPbBr_3$ QDs, and lowers production costs. Nonetheless, the higher toxicity of PbO compared to PbBr poses a challenge, and the redox implications during the melting process may result in color instability in the glass, thus detrimentally affecting the luminescent properties of $CsPbBr_3$ QDs and hindering large-scale production of $CsPbBr_3$ QDs@glass. Introducing Pb^{2+} as an extrinsic component into the glass matrix can partially alleviate its viscosity and optimize the glass structure. However, the large radius and high charge of Pb^{2+} exert a strong gravitational force on surrounding tetrahedral structures such as $[SiO_4]$ and $[BO_4]$[25], rendering the glass structure more densely packed, consequently impacting the luminescent intensity of $CsPbBr_3$ QDs. Although there is still a need for further investigation into the influence of Pb^{2+} on the structure of $CsPbBr_3$ QDs@glass, substantial findings regarding the overall impact of Pb^{2+} on glass have been accumulated[26-29]. Building upon a comprehensive understanding of these strategies, future discourse can delve deeper into the effects of Pb^{2+} on the structure of $CsPbBr_3$ QDs@glass.

Herein, $CsPbBr_3$ QDs@glass were fabricated employing a melt-anneal approach. Delving into the thermal induction temperature, an in-depth exploration was conducted to investigate the influence of Pb^{2+} on the structural characteristics of $CsPbBr_3$ QDs@glass, while simultaneously refining and optimizing the PL intensity of $CsPbBr_3$ QDs@glass. On this basis, the potential applications of $CsPbBr_3$ QDs@glass in the domains of LED lighting and displays were systematically explored. These endeavors laid a solid foundation for the large-scale production of $CsPbBr_3$ QDs@glass and significantly expanded their practical implementations in the realms of LED illumination and display technologies.

1 Experimental

1.1 Chemicals

Silica (SiO_2, 99.95%) was purchased from Xinyi Dahan Mining Co., Ltd. Boric acid (B_2O_3, 99%) was purchased from Sinopharm Chemical Reagent Co., Ltd. Zinc oxide (ZnO, 99%), calcium fluoride (CaF_2), cesium carbonate (Cs_2CO_3, 99%), lead Bromide ($PbBr_2$), sodium bromide (NaBr,), lead oxide (PbO) were purchased from Aladdin Biochemical Technology Corp. All chemicals were used without any further purification.

1.2 Fabrication of $CsPbBr_3$ QDs @glass

In this work, the glass composition consists of: $85SiO_2$-$170H_3BO_3$-55ZnO-$5CaF_2$-$16Cs_2CO_3$-$5PbBr_2$-15NaBr-0.5PbO. 40 g of the above raw materials were weighed and poured into a mixing tank for 2 h mixing at 25 Hz. The mixed raw materials were poured into the preheated platinum crucible, and then the lid was closed. Subsequently, all raw materials were melted in a high-temperature electric furnace at 1250 ℃ for 30 min. Afterward, the melted glass was poured into a preheated steel mold at 370 ℃ so that the molten glass can be formed. Whereafter, the formed glass was returned to the muffle furnace at 370 ℃ for removal of stress. At this point, the precursor glass was obtained. Precursor glass was heat treated by crystallization furnace in the range of 440 ℃ to 510 ℃ for 2 h. Finally, $CsPbBr_3$ QDs@glass was obtained. The preparation steps were illustrated in Fig. 1.

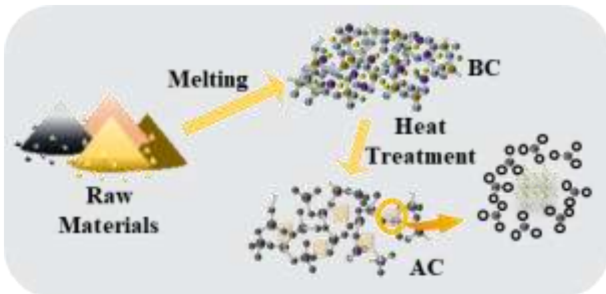

Fig. 1 Schematic of preparation of quantum dot glass-ceramics
AC: After Crystallization; BC: Before Crystallization

1.3 Structural Characterization

X-ray diffraction system (XRD, D/max 2550V, RIGAKU, Japan) with Cu Kα radiation (λ=0.1542 nm) is used to detect the phase structure of $CsPbBr_3$ crystals. Transmission electron microscopy (TEM, JEM-2100F, JEOL, Japan) with energy dispersive X-ray (EDX) is used to observe the microscopic morphology and size of a sample. Fourier Transform Infrared Spectroscopy (FTIR, EQUINOX55, Bruker, Germany) was used to test the structure of glass. X-ray Photoelectron Spectroscopy (XPS, Escalab250Xi, Thermo Fisher, China) was used to test the components and Changes in non-bridging oxygen bonds. The samples used for testing were all in powder state.

1.4 Optical Characterization

The PL spectra, and PLQY were recorded by a steady-state transient fluorescence spectrometer (PL, Fluorolog-3, HORIBA, Japan). The steady-state measurement system adopts a 450 w continuous xenon lamp and CCD detector, and the transient measurement system adopts a new high-frequency pulse light source and a 980 nm pulse width continuous adjustable laser. When carrying out the spectrum test with an excitation wavelength of 365 nm, the integration time is selected as 5 s, meanwhile, excitation light slit width was 3 nm, emission light slit width is 2 nm, and the test range is 450 nm to 600 nm. All samples were powder state.

1.5 Fabrication and Testing of LED Device

The LED device was prepared by 2 g of PDMS with a molar ratio of $CsPbBr_3$ QDs@glass powder, and n(powder):n(PDMS) = 1:32. In order to mix evenly, the powder was magnetically stirred with PDMS for 2 h. Subsequently, the powder-glue mixture was dropped onto a 365 nm UV chip, and finally a green LED was obtained. The optical performance test of LED devices uses a comprehensive optical performance characterization system (Varian, English). During the test, a power supply with a power of 3 W to 5 W was used.

2 Results and discussion

To investigate the influence of heat treatment on QDs microcrystalline glass and establish an optimal thermal processing protocol for subsequent research, this study initially obtained a pristine and transparent borosilicate glass precursor under the melting conditions of 1250 ℃ for 30 min. Subsequently, under the condition of a 2 h thermal induction time, heat treatment was conducted on the glass precursor, and the results for thermal induction temperatures ranging from 440 ℃ to 510 ℃ were shown in Fig. 2.

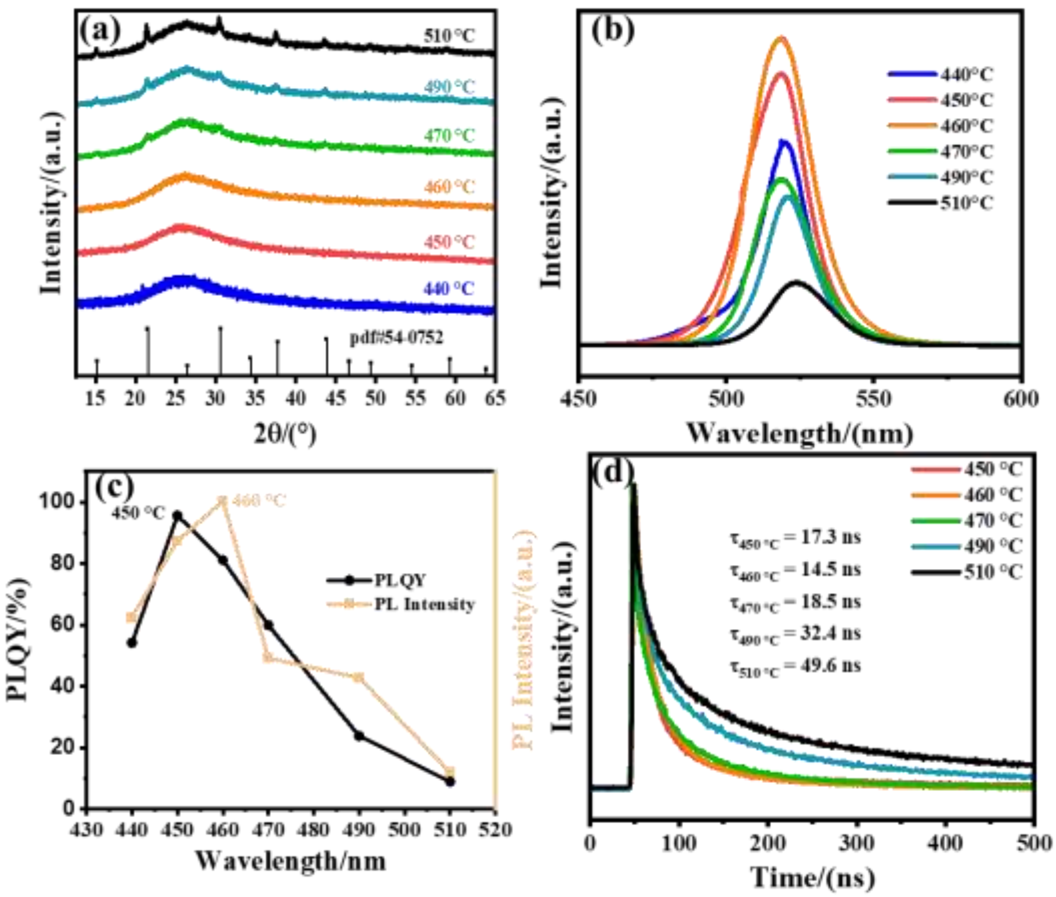

Fig.2 Characterization of the structure and optical properties of PQDs @glass at different temperatures under 2 h

(a) XRD; (b) PL spectra; (c) PLQY and PL intensity and (d) Fluorescence lifetime curve

Fig. 2(a) exhibits the XRD spectra of $CsPbBr_3$

QDs@glass obtained under the conditions of a 2 h thermal induction time and temperatures ranging from 440 ℃ to 510 ℃. The data in the graph were compared with pdf#54-0752, indicating successful synthesis of $CsPbBr_3$ QDs@glass at different temperatures. Moreover, as the temperature was elevated, the crystalline peaks became more pronounced.

Subsequently, fluorescence spectroscopy was performed to characterize the samples at different temperatures, and the results are shown in Fig. 2(b-d). Fig. 2(b) depicts the PL spectrum, revealing a noticeable redshift in the emission center as the temperature increases. To investigate the underlying cause, TEM characterization was conducted, and the size distribution of $CsPbBr_3$ QDs at different temperatures was analyzed (Fig. 3(g-k)). The results demonstrate a gradual increase in the size of $CsPbBr_3$ QDs with rising temperature. At 450 ℃, the QDs predominantly have a size distribution around 5 nm. In the temperature range of 460 ℃ to 490 ℃, with over 86% of the particles falling within the size range of 6-14 nm. When the temperature reaches 510 ℃, the size distribution centers around 40 nm. This observed redshift in the emission center can be explained by the quantum size effect, where the bandgap of QDs decreases as their size increases (illustrated in Fig. 3(f)).

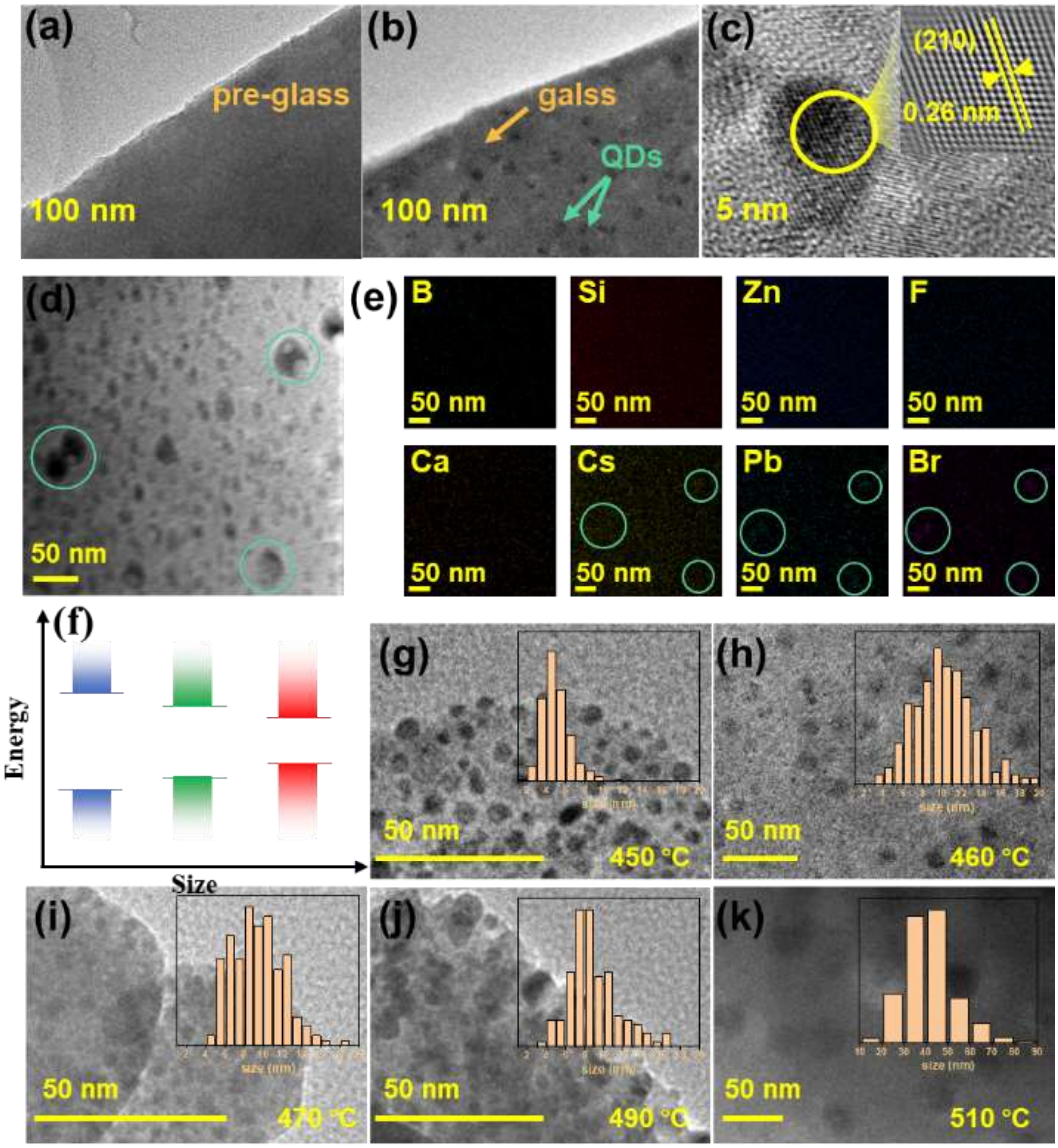

Fig. 3 TEM characterization and size distribution analysis of PQDs @glass

(a-b) TEM images before and after heat treatment; (c) High-resolution TEM image and (d-e) TEM images and mapping; (f) Schematic diagram of the relationship between size and band gap of $CsPbBr_3$ QDs and (g-k) TEM images and size statistics

Furthermore, the TEM images clearly indicate that the quantity of QDs increases within the temperature range of 450 ℃ to 490 ℃. Initially, during the nucleation stage, the increased number of QDs leads to enhanced PL intensity and PLQY. However, as the number of QDs continues to increase, self-absorption becomes more pronounced, resulting in a decrease in PL intensity and PLQY (as shown in Fig. 2(b, c)). Additionally, the fluorescence spectra demonstrate that the highest PL intensity is achieved at 460 ℃, while the PLQY reaches a peak value of 95.6% at 450 ℃.

What follows is a further exploration of the microstructure of $CsPbBr_3$ QDs@glass, as shown in Fig. 3(a-e). Additional evidence of the successful synthesis of $CsPbBr_3$ QDs within the borosilicate glass matrix is provided by Fig. 2(a-c). Particularly, the high-resolution TEM image (Fig. 3(c)) reveals an interlayer spacing of 0.26 nm, corresponding to the (210) crystal plane of $CsPbBr_3$ QDs. The mapping images in Fig. 3(d-e) illustrate the accumulation of Cs^+, Pb^{2+}, and Br^- ions within the region where the QDs precipitate. This observation aligns with previous studies suggesting that the abundance of Cs^+ contributes to the formation of $CsPbBr_3$ QDs.

With the goal of enhancing luminescence intensity, this study further investigates the influence of Pb^{2+} ions on the structure of $CsPbBr_3$ QDs@glass, building upon the aforementioned research. The regulation of Pb^{2+} ion composition is presented in Table 1.

This resulted in a tighter glass structure and increased density. Pb^{2+} ions were able to form more bond connections within the glass network, which contributed to strengthening the three-dimensional network structure of the glass. Due to the higher charge and larger ion radius of Pb^{2+}, it exerted a strong attractive force on the surrounding [SiO_4] and [BO_4], stabilizing the entire network structure. The decreased transparency from Pb-1 to Pb-4 further supported this observation. As a direct consequence, the glass precursor of Pb-1 formed a looser structure, facilitating the migration of Cs^+, Pb^{2+}, and Br^- ions during annealing and stress relaxation processes, thus resulting in crystallization. With the increasing concentration of Pb^{2+} ions, the density of the glass gradually increased. However, when it exceeded a certain range, it led to the formation of more interfaces within the precursor. These interfaces lowered the energy barrier for the formation of nanocrystals by Cs^+, Pb^{2+}, and Br^- ions. Therefore, a small portion of crystals reappeared in the precursors of Pb-3 and Pb-4.

Fig. 4(a) presents the glass precursors prepared with different conditions of Pb^{2+} ions. The results indicated that extensive crystallization did not occur in Pb-2, Pb-3, and Pb-4 precursors, whereas Pb-1 precursor exhibited crystal formation due to the larger radius of Pb^{2+} ions that occupied more space in the lattice structure and increased the atomic packing density of the glass.

The XRD results after thermal induction at 460 ℃ for 2 h (Fig. 4(b)) aligned with the precursor results (Fig. 4(a)). The presence of a significant number of crystals in the Pb-1 precursor acted as favorable nucleation sites during the subsequent thermal induction process, promoting the formation of $CsPbBr_3$ QDs within the borosilicate glass. The higher intensity of the crystalline peaks in Pb-1, relative to Pb-2, Pb-3, and Pb-4, further substantiates this observation.

Table 1 Component regulation of Pb^{2+} ions (all data in molar ratios)

Code	SiO_2	H_3BO_3	ZnO	CaF_2	Cs_2CO_3	$PbBr_2$	NaBr	PbO
Pb-1	85	170	55	5	16	4	17	0.5
Pb-2	85	170	55	5	16	5	15	0.5
Pb-3	85	170	55	5	16	6	13	0.5
Pb-4	85	170	55	5	16	7	11	0.5

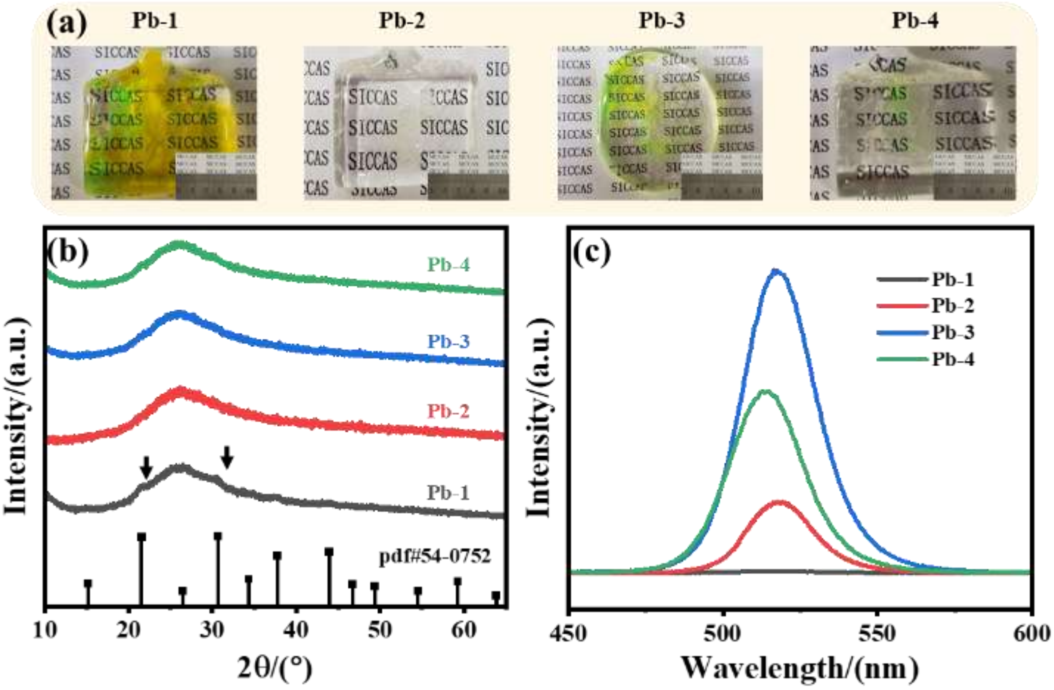

Fig. 4 (a) Photograph, (b) XRD and (c) PL spectra of $CsPbBr_3$ QDs @glass at different Pb^{2+} concentrations

At this stage, the luminescent performance of the samples was characterized, and it was observed that Pb-3 exhibited the optimal results. This indicates that an inadequate concentration of Pb^{2+} in the precursor led to the occurrence of uncontrollable crystallization, resulting in a reduction in the final PL intensity. Likewise, an excessive concentration of Pb^{2+} resulted in a high density of the borosilicate glass precursor, which hindered the migration of Cs^+, Pb^{2+}, and Br^- ions necessary for the formation of $CsPbBr_3$ QDs. Consequently, this excessive density contributed to a decrease in PL intensity.

To investigate the impact of Pb^{2+} ions on the luminescent properties of $CsPbBr_3$ QDs in glass, we further employed Fourier-transform infrared spectroscopy and X-ray photoelectron spectroscopy to delve into the glass structure. The results are shown in Fig. 5(a-c). Fig. 5(a) illustrates that the glass network structure is primarily composed of polyhedra such as [BO_3], [BO_4], and [SiO_4]. The peak at 710 cm^{-1} corresponds to the bending vibration of B−O bonds in the [BO_3] groups. The broad peak at 1024 cm^{-1} corresponds to the stretching vibrations of both [BO_4] groups and Si−O−Si bonds. The shoulder peak at 1272 cm^{-1} corresponds to the vibration of [BO_3] polyhedra, while the shoulder peak at 1375 cm^{-1} corresponds to the asymmetric stretching vibration of [BO_3] polyhedra.

From Pb-1 to Pb-4, a broad peak at 1024 cm^{-1} noticeably shifts towards higher wavenumbers, indicating an increasing content of [SiO_4] and [BO_4]. This suggests that the glass network structure becomes more compact with the increasing concentration of Pb^{2+}. It aligns well with our previous speculation regarding the occurrence of uncontrolled crystallization in the precursor. Moreover, through XPS analysis, we investigated the ratio of bridging oxygen bonds to non-bridging oxygen bonds in the borosilicate glass (Fig. 5(c)). The results indicate that the proportion of bridging oxygen bonds gradually increases as the Pb^{2+} concentration rises. This explains the aforementioned hypothesis that "Pb^{2+} exerts a stronger attraction on neighboring [SiO_4] and [BO_4], contributing to the enhancement of the three-dimensional network structure of the glass."

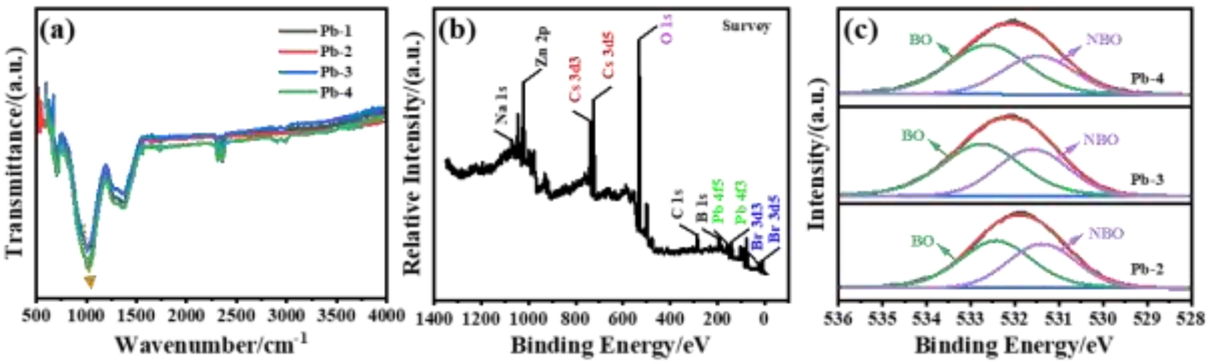

Fig. 5 Structural characterization of PQDs@glass at different Pb^{2+} concentrations

(a-b) FT-IR and XPS spectra and (c) the ratio of bridging and non-bridging oxygen bonds

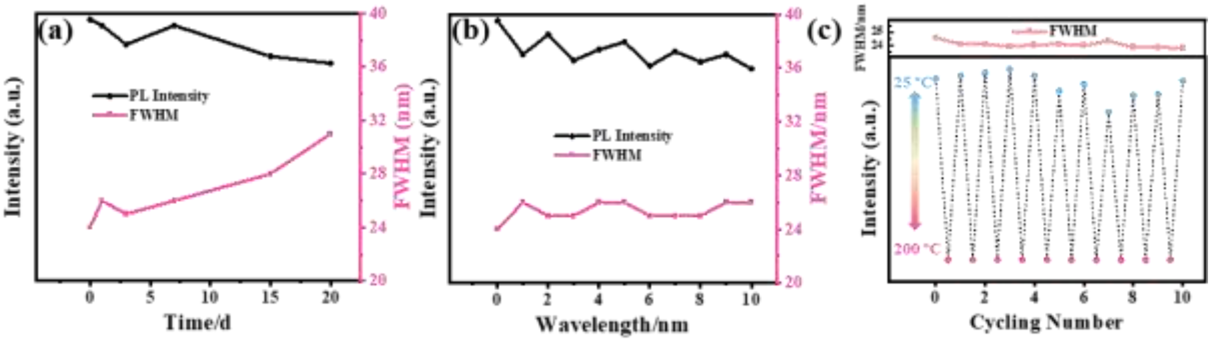

Fig. 6 Stability experiments of PQDs @glass

(a-b) Variations in PL intensity and FMHW of water resistance and UV stability, and (c) experimental results of thermal cycling stability

Subsequently, this study evaluated the water resistance, UV irradiation resistance, and thermal cycling stability of the samples. The results indicate that the luminescence intensity can maintain over 70% of its initial value even after immersion for 360 h (as depicted in Fig. 6(a)). Similarly, the luminescence intensity remained above 70% of its initial value after exposure to UV radiation for 210 h (as illustrated in Fig. 6(b)). The primary reasons for the attenuation of its water stability and UV stability are mainly due to the fact that during the high-energy ball milling process, the powder material develops numerous cracks, resulting in a greater number of QDs being exposed. Consequently, these exposed QDs are more susceptible to environmental influences, which lead to a significant decrease in their intensity. And after undergoing 10 cycles of thermal cycling, the luminescence intensity of $CsPbBr_3$ QDs@glass retained 98.9% of its initial value without significant decrease. The luminescence intensity for each individual cycle maintained over 80% of its initial value. Moreover, the FWHM was relatively stable at around 24 nm, without significant change (as demonstrated in Fig. 6(c)).

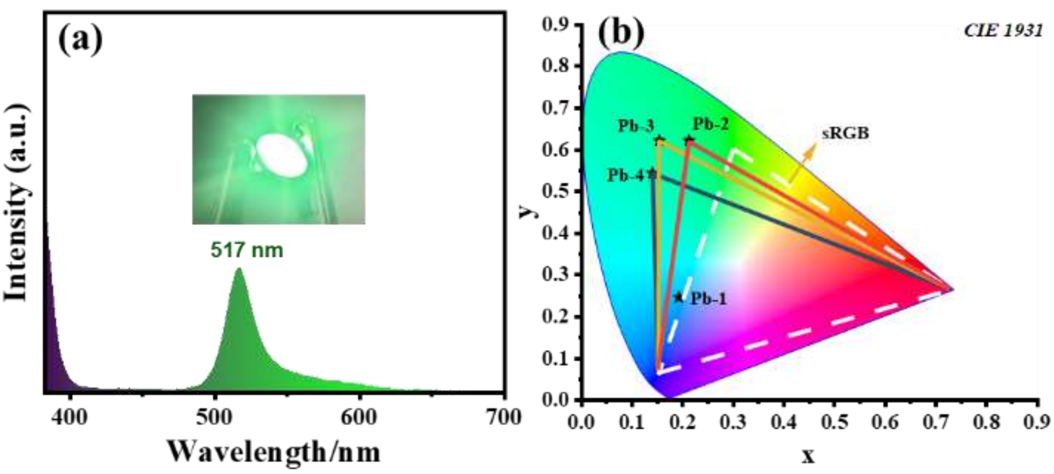

Fig.7 (a) LED device fabricated with $CsPbBr_3$ QDs @glass, and (b) CIE coordinates of $CsPbBr_3$ QDs @glass LED devices at different Pb^{2+} concentrations

Finally, the material was mixed with PDMS and combined with a 365 nm UV chip to create LED microspheres. The characterization results, depicted in Fig. 7(a), show that the LED samples produced using Pb-2 as the base material under thermal induction conditions of 460 ℃ for 2 h have an emission center at 517 nm (Fig. 2(b)), closely matching the original material's emission center at 518 nm. Additionally, Fig. 7(b) reveals that the LED color coordinates achieved with Pb-2, Pb-3, and Pb-4 were (0.21, 0.62), (0.16, 0.60), and (0.14, 0.53) respectively, encompassing a spectrum of 110% sRGB color gamut and extending the boundaries of color space.

3 Conclusion

This study examined the relationship between thermal induction temperature and the bandgap of $CsPbBr_3$ QDs. By optimizing the thermal induction temperature to 460 ℃, researchers investigated how Pb^{2+} ions affected the luminescent properties of $CsPbBr_3$ QDs@glass. The results led to the continuous improvement of PL intensity and a high PLQY of up to 95.6% for $CsPbBr_3$ QDs@glass. LED devices were then fabricated from these materials, which resulted in an expanded standard RGB color gamut. This research has extended the potential applications of $CsPbBr_3$ QDs@glass in the domains of LED lighting and displays, laying a fundamental basis for the large-scale fabrication of $CsPbBr_3$ QDs@glass.

Acknowledgements

The authors acknowledge funding sponsored by the Hengdian Group Holding Co. LTD. This research work was supported by the joint fund from Hengdian Group and Shanghai Institute of Ceramics, Chinese Academy of Sciences.

References

[1] SU W, TENG Q, YUAN F. All-thermally evaporated perovskite LEDs toward high-resolution active-matrix displays. *Matter*, 2023, **6(8):** 2539.

[2] KIM D, PARK S, CHOI B C, *et al.* The tetravalent manganese activated $SrLaMgTaO_6$ phosphor for w-LED applications. *Materials Research Bulletin*, 2018, **97:** 115.

[3] CHRISTENSEN A, GRAHAM S. Thermal effects in packaging high power light emitting diode arrays. *Applied Thermal Engineering*, 2009, **29(2/3):** 364.

[4] WEN Z, XIE F, CHOY W C H. Stability of electroluminescent perovskite quantum dots light - emitting diode. *Nano Select*, 2021, **3(3):** 505.

[5] WANG S, BI C, YUAN J, *et al.* Original core–shell structure of cubic $CsPbBr_3$@Amorphous $CsPbBr_x$ perovskite quantum dots with a high blue photoluminescence quantum yield of over 80%. *ACS Energy Letters*, 2017, **3(1):** 245.

[6] RAIN G, YAZDANI N, BOEHME S C, *et al.* Ultra-narrow room-temperature emission from single $CsPbBr_3$ perovskite quantum dots. *Nature Communications*, 2022, **13(1):** 2587.

[7] ZHOU X, CHANG Q, XIANG G, *et al.* A and B sites dual substitution by Na^+ and Cu^{2+} co-doping in $CsPbBr_3$ quantum dots to achieve bright and stable blue light emitting diodes. *Spectrochimica Acta Part A: Molecular and Biomolecular Spectroscopy*, 2023, **300:** 122773.

[8] WU W, ZHAO C, HU M, *et al.* $CsPbBr_3$ perovskite quantum dots grown within Fe-doped zeolite X with improved stability for sensitive NH_3 detection. *Nanoscale*, 2023, **15(12):** 5705.

[9] LIN C Q, LIU M L, YANG Z, *et al.* Mn^{2+} doped $CsPbBr_3$ perovskite quantum dots with high quantum yield and stability for flexible array displays. *Journal of Solid State Chemistry*, 2023, **327:** 124295.

[10] LIU S, SHAO G, DING L, *et al.* Sn-doped $CsPbBr_3$ QDs glasses with excellent stability and optical properties for WLED. *Chemical Engineering Journal*, 2019, **361:** 937.

[11] HUANG D, BO J, ZHENG R, *et al.* Luminescence and stability enhancement of $CsPbBr_3$ perovskite quantum dots through surface sacrificial coating. *Advanced Optical Materials*, 2021, **9(16):** 2100474.

[12] ZOU L, LI X, YANG M, *et al.* ZnPc/$CsPbBr_3$ QDs collaborative interface modification to improve the performance of $CsPbBr_3$ perovskite solar cells. *Solar Energy Materials and Solar Cells*, 2023, **251:** 112157.

[13] XU Y, YU L, PENG K, *et al.* Ultra - stable perovskite quantum dot composites encapsulated with mesoporous SiO_2 and PbBr(OH) for white light - emitting diodes. *Luminescence*, 2023, **38(5):** 536.

[14] REN J, LI T, ZHOU X, *et al.* Encapsulating all-inorganic perovskite quantum dots into mesoporous metal organic frameworks with significantly enhanced stability for optoelectronic applications. *Chemical Engineering Journal*, 2019, **358:** 30.

[15] LV W, LI L, XU M, *et al.* Improving the stability of metal halide perovskite quantum dots by encapsulation. *Advanced Materials*, 2019, **31(28):** 1900682.

[16] LI S, NIE L, MA S, *et al.* Environmentally friendly $CsPbBr_3$ QDs multicomponent glass with super-stability for optoelectronic devices and up-converted lasing. *Journal of the European Ceramic Society*, 2020, **40(8):** 3270.

[17] YANG B, MEI S, ZHU Y, *et al.* Precipitation promotion of highly emissive and stable $CsPbX_3$ (Cl, Br, I) perovskite quantum dots in borosilicate glass with alkaline earth modification. *Ceramics International*, 2023, **49(4):** 6720.

[18] TONG Y, WANG Q, LIU X, *et al.* The promotion of TiO_2 induction for finely tunable self-crystallized $CsPbX_3$(X = Cl, Br and I) nanocrystal glasses for LED backlighting display. *Chemical Engineering Journal*, 2022, **429:** 132391.

[19] SHAO G, LIU S, DING L, *et al.* $K_xCs_{1-x}PbBr_3$ NCs glasses possessing super optical properties and stability for white light emitting diodes. *Chemical Engineering Journal*, 2019, **375:** 122031.

[20] LIU S, HE M, DI X, *et al.* Precipitation and tunable emission of cesium lead halide perovskites ($CsPbX_3$, X = Br, I) QDs in borosilicate glass. *Ceramics International*, 2018,

44(4): 4496.

[21] LIU J, SHEN L, CHEN Y, *et al.* Highly luminescent and ultrastable cesium lead halide perovskite nanocrystal glass for plant-growth lighting engineering. *Journal of Materials Chemistry C*, 2019, **7(43):** 13606.

[22] STOCH P, STOCH A. Structure and properties of Cs containing borosilicate glasses studied by molecular dynamics simulations. *Journal of Non-Crystalline Solids*, 2015, **411:** 106.

[23] LIU Q, FENG L, SUN Y, *et al.* Effects of phosphate glass on Cs^+ immobilization in geopolymer glass-ceramics. *Ceramics International*, 2023, **49(4):** 6545.

[24] YANG B, MEI S, HE H, *et al.* Lead oxide enables lead volatilization pollution inhibition and phase purity modulation in perovskite quantum dots embedded borosilicate glass. *Journal of the European Ceramic Society*, 2022, **42(1):** 258.

[25] KAUR N, KHANNA A, G NZ LEZ-BARRIUSO M, *et al.* Effects of Al^{3+}, W^{6+}, Nb^{5+} and Pb^{2+} on the structure and properties of borotellurite glasses. *Journal of Non-Crystalline Solids*, 2015, **429:** 153.

[26] OTHMAN H, TOPPER B, ELKHOLY H, *et al.* Structural, spectroscopic, and radiation shielding properties of Pb^{2+}-doped borate and phosphate glasses. *International Journal of Applied Glass Science*, 2023, **14(3):** 408.

[27] LI P, TIAN Y, HUANG F, *et al.* Highly efficient photostimulated luminescence of Pb^{2+} doped $SrAl_2O_4:Eu^{2+}$, Dy^{3+} borate glass for long-term stable optical information storage. *Journal of the European Ceramic Society*, 2022, **42(12):** 5065.

[28] EL-EGILI K, DOWEIDAR H, MOUSTAFA Y M, *et al.* Structure and some physical properties of $PbO–P_2O_5$ glasses. *Physica B: Condensed Matter*, 2003, **339(4):** 237.

[29] CHENG Y, XIAO H, GUO W, *et al.* Structure and crystallization kinetics of $PbO–B_2O_3$ glasses. *Ceramics International*, 2007, **33(7):** 1341.

Pb^{2+}对掺杂硼硅酸盐玻璃中 $CsPbBr_3$ 钙钛矿量子点发光性能的影响

岳仔豪[1,2]，杨小兔[1]，张正亮[1]，邓瑞翔[1]，张 涛[1]，宋力昕[1,2]

(1. 中国科学院 上海硅酸盐研究所，上海 200050; 2. 上海科技大学 物质科学与技术学院，上海 201210)

摘 要: 硼硅酸盐玻璃包覆钙钛矿 $CsPbBr_3$ 量子点(PQDs)能够大大提高 PQDs 的稳定性，这使得它在 LED 照明和显示技术中拥有广泛的应用空间。然而，玻璃包覆同时也导致了 PQDs 发光强度与其量子产率的降低。本工作通过探讨热诱导温度及 Pb^{2+}的含量对钙钛矿 $CsPbBr_3$ 量子点微晶玻璃(PQDs@glass)结构的影响，极大地提高了 PQDs@glass 的发光强度并得到量子产率高达 95.6%的 PQDs @glass。同时，本工作实现了硼硅酸盐玻璃基质内 PQDs 的尺寸可控制备，结果表明，PQDs 尺寸分布在 10 nm 左右，超过 86%的颗粒尺寸在 6~14 nm 内，且其具有优越的稳定性，经历 10 次室温至 200 ℃热循环后，其仍能保持初始强度的 98.9%。最后，为了验证其在 LED 照明及显示领域的应用，本课题组将得到的量子点微晶玻璃粉料与二甲基硅氧烷(PDMS)混合，得到色域范围覆盖 110% sRGB 的优异 LED 器件。这为钙钛矿量子点微晶玻璃的大规模制备及其在 LED 器件领域的应用奠定了基础。

关 键 词: $CsPbBr_3$；Pb^{2+}；LED；量子点；硼硅酸盐玻璃

中图分类号: TQ174 **文献标志码**: A